

Regional Asymmetries in Ocean Heat and Carbon Storage due to Dynamic Redistribution in Climate Model Projections

RICHARD G. WILLIAMS,^a ANNA KATAVOUTA,^{a,b} AND VASSIL ROUSSENOV^a

^a *Department of Earth, Ocean and Ecological Sciences, School of Environmental Sciences, University of Liverpool, Liverpool, United Kingdom*

^b *National Oceanography Centre, Liverpool, United Kingdom*

(Manuscript received 7 July 2020, in final form 30 January 2021)

ABSTRACT: Projected changes in ocean heat and carbon storage are assessed in terms of the added and redistributed tracer using a transport-based framework, which is applied to an idealized climate model and a suite of six CMIP5 Earth system models following an annual 1% rise in atmospheric CO₂. Heat and carbon budgets for the added and redistributed tracer are used to explain opposing regional patterns in the storage of ocean heat and carbon anomalies, such as in the tropics and subpolar North Atlantic, and the relatively reduced storage within the Southern Ocean. Here the added tracer takes account of the net tracer source and the advection of the added tracer by the circulation, while the redistributed tracer takes account of the time-varying circulation advecting the preindustrial tracer distribution. The added heat and carbon often have a similar sign to each other with the net source usually acting to supply the tracer. In contrast, the redistributed heat and carbon consistently have an opposing sign to each other due to the opposing gradients in the preindustrial temperature and carbon. These different signs in heat and carbon redistribution can lead to regional asymmetries in the climate-driven changes in ocean heat and carbon storage. For a weakening in the Atlantic overturning and strengthening in the Southern Ocean residual circulation, the high latitudes are expected to have heat anomalies of variable sign and carbon anomalies of a consistently positive sign, since added and redistributed tracers are opposing in sign for heat and the same sign for carbon there.

KEYWORDS: Meridional overturning circulation; Upwelling/downwelling; Anthropogenic effects/forcing; Climate change; Climate models

1. Introduction

The ocean provides an important role in sequestering the extra carbon and heat supplied to the climate system from carbon emissions and the rise in radiative forcing. This additional heat and carbon is preferentially stored in the upper ocean, residing mainly within the mixed layer and the stratified thermocline (Sabine et al. 2004; Zanna et al. 2019).


The relationship between the patterns of climate-driven changes in heat and carbon storage varies according to their surface sources and sinks and the controlling dynamics. The additional heat and carbon supplied to the surface mixed layer spreads into the rest of the ocean following ventilation pathways, involving subduction into the thermocline or convective transfer to the deep ocean, as part of a combination of gyre, eddy, and overturning circulations. Accordingly, the storage of the extra heat and carbon might be expected to mimic each other given their similar ventilation pathways. However, there are differences in this heat and carbon storage due to contrasts in their surface sources and sinks: the supply of heat is affected by air–sea transfer processes and radiative feedbacks, while the supply of carbon is affected by air–sea transfer processes, solubility changes, and buffering from carbonate chemistry and is weakly modified by biological cycling.

The climate-driven changes in ocean heat and carbon storage are also affected by how the time-varying circulation redistributes

pre-existing heat and carbon in the ocean, as well as by the addition of heat and carbon. This redistribution effect is more prominent for heat than carbon due to the relatively large latitudinal and depth contrasts in temperature compared with the more limited contrasts for dissolved inorganic carbon (Winton et al. 2013).

The resulting patterns of the climate-driven changes in heat and carbon storage might then be expected to fall within one of two regimes: (i) similar patterns in heat and carbon gain if the added heat and carbon spread passively along the same ventilation pathways and differing only due to differences in their surface sources or (ii) contrasting patterns in heat and carbon gain if the time-varying circulation drives significant redistribution of pre-existing heat and carbon.

In accord with these different regimes, there are different explanations for the climate-driven changes in ocean heat and carbon storage. Anthropogenic heat is often viewed as spreading in a passive manner, as mapped over the globe by Zanna et al. (2019), and used to explain how heat sequestered in the Southern Ocean (Frölicher et al. 2015) spreads northward, advected by the preindustrial circulation (Marshall et al. 2015; Armour et al. 2016). However, anthropogenic heat is also viewed to evolve in a dynamical manner in the North Atlantic, taking into account the effect of a temporal change in the circulation (Banks and Gregory 2006; Xie and Vallis 2012; Winton et al. 2013; Gregory et al. 2016). Both of these passive and dynamic effects are taken into account in how the anthropogenic

 Denotes content that is immediately available upon publication as open access.

Corresponding author: Richard G. Williams, ric@liverpool.ac.uk

DOI: 10.1175/JCLI-D-20-0519.1



This article is licensed under a [Creative Commons Attribution 4.0 license](http://creativecommons.org/licenses/by/4.0/) (<http://creativecommons.org/licenses/by/4.0/>).

TABLE 1. Global metrics for six CMIP5 Earth system models forced by an annual 1% rise in atmospheric CO₂ after 100 years: global-mean increase in upper ocean temperature T' and carbon DIC' relative to the preindustrial evaluated over the upper 500 m, a comparison between the ratios of depth contrasts in the preindustrial tracer and anthropogenic tracer, $\Delta T_o/\Delta T'$ and $\Delta \text{DIC}_o/\Delta \text{DIC}'$, where the tracer contrasts $\Delta c = c(z_1) - c(z_2)$ are taken as the magnitude in the tracer difference across the thermocline (between the upper 500 m and from below the depth of 2500 m). The dynamic redistribution is relatively large for temperature compared to carbon, as the ratios of $\Delta T_o/\Delta T'$ are greater than that of $\Delta \text{DIC}_o/\Delta \text{DIC}'$ from (5). The upper three models have a stronger Atlantic overturning, while the lower three models have a weak overturning.

Earth system model	T' (K)	DIC' (mmol m ⁻³)	$\Delta T_o/\Delta T'$	$\Delta \text{DIC}_o/\Delta \text{DIC}'$	$(\Delta T_o/\Delta T')/(\Delta \text{DIC}_o/\Delta \text{DIC}')$	Reference
GFDL-ESM2M	0.77	111	13.6	-1.9	-7.1	Dunne et al. (2013)
NorESM1-ME	1.01	112	10.6	-0.7	-16.0	Tjiputra et al. (2013)
MPI-ESM-LR	1.19	119	8.9	-1.5	-5.9	Giorgetta et al. (2013)
HadGEM2-ES	1.27	116	7.6	-1.5	-5.2	Jones et al. (2011)
CanESM2M	1.35	112	7.7	-1.2	-6.5	Arora et al. (2011)
IPSL-CM5A-LR	1.37	125	7.8	-1.7	-4.5	Dufresne et al. (2013)

heat is viewed in terms of added and redistributed heat components (Xie and Vallis 2012; Gregory et al. 2016).

The ocean carbon is often separated into anthropogenic carbon and a much larger background of natural carbon. The anthropogenic carbon is usually diagnosed from observations using a quasi-conserved carbon tracer (Gruber et al. 1996; Sabine et al. 2004; Clement and Gruber 2018) or inferred from recently injected anthropogenic tracers, such as CFCs, assuming an unchanging ocean circulation (Hall et al. 2002; Waugh et al. 2006; Khatiwala et al. 2009; DeVries 2014). The time-varying circulation alters the transport of anthropogenic carbon (DeVries et al. 2017; Gruber et al. 2019), as well as leading to the redistribution of the natural carbon (Bernardello et al. 2014; Thomas et al. 2018). In addition, a carbon-cycle feedback framework is used to separate changes in the global ocean carbon inventory into contributions from the increase in atmospheric CO₂ or from changes in physical climate, where the physical climate combines together the effects of warming and circulation changes (Friedlingstein et al. 2006; Schwinger et al. 2014; Williams et al. 2019; Arora et al. 2020).

The extent to which the patterns of climate-driven changes in ocean heat and carbon storage resemble each other is first illustrated for centennial projections of six CMIP5 Earth system models following a 1% annual rise in atmospheric CO₂ (section 2). The changes in ocean heat and carbon storage are explored using the same transport-based framework, separating the tracer storage into contributions from the added tracer and redistributed tracer (section 3). The ocean heat and carbon responses are compared using a simplified climate model for the Atlantic sector with and without a changing overturning (section 4). The transport-based framework is then applied to identify the added and redistributed heat and carbon for the CMIP5 Earth system models (section 5) for three regions experiencing different dynamic responses: the subpolar North Atlantic, the tropical Atlantic, and the Southern Ocean. The wider implications of the study are finally discussed (section 6).

2. Regional variations in the change in ocean heat and carbon storage in CMIP5 projections

The changes in upper ocean heat and carbon storage are considered for projections following an annual 1% rise in atmospheric

CO₂ over 140 years for six CMIP5 Earth system models (Table 1). All the models follow the same atmospheric CO₂ history starting from a preindustrial value of 286 ppm, which is increased by 1% every year and reaches 750 ppm at year 100.

All of the models reveal widespread projected increases in global ocean heat and carbon storage, varying from 1.4×10^{24} to 1.9×10^{24} J and from 350 to 460 PgC, respectively, which are much larger than the historical increases from the preindustrial to the present day of typically 4.36×10^{21} J (Zanna et al. 2019) and 160 PgC (Friedlingstein et al. 2020). Over the Atlantic sector, the increase in ocean heat and carbon occurs mainly over the upper kilometer, coinciding with the thick thermocline over the subtropical gyres, typically at 40°S and 40°N (Figs. 1a,b; see also Figs. A1a,b in the appendix).

A normalized tracer anomaly is used to compare the regional patterns in ocean heat and carbon storage, which is positive or negative according to whether the local tracer storage is greater or less than the global mean. The normalized tracer, $(c' - \langle c' \rangle)/\sigma_{c'}(t)$, is defined by the actual tracer anomaly minus the global-mean tracer anomaly, divided by the standard deviation over the global domain; here the prime indicates the local change in tracer since the preindustrial, where $c(x, y, z, t) = c_o(x, y, z, t_o) + c'(x, y, z, t)$ (c_o is the preindustrial tracer at time t_o and c' is the tracer anomaly in time), and the angle brackets indicate a volume-weighted, global mean, $\langle c'(t) \rangle = (1/V) \int_V c'(x, y, z, t) dV$, where V is the volume, and $\sigma_{c'}$ is the standard deviation of c' over the global domain.

The normalized thermal anomaly reveals generally a preferential heat storage in the subtropics and the tropics in the Atlantic, but sometimes a reduction in heat storage in the subpolar North Atlantic relative to the global mean (Fig. 1c). The normalized carbon anomaly reveals a more consistent response with enhanced carbon storage in the middle and high latitudes of the North Atlantic and the subtropics of the Southern Hemisphere, but less carbon storage in the tropics for most models relative to the global mean (Fig. 1d).

The relationship between the normalized heat and carbon anomalies is particularly variable over the Atlantic domain (Figs. 1c,d), and there are smaller differences in the Pacific and Indian basins. Over the subtropics, the enhanced storage of heat and of carbon are often consistent with each other. However, over the tropics, there is usually an increase in heat storage relative to

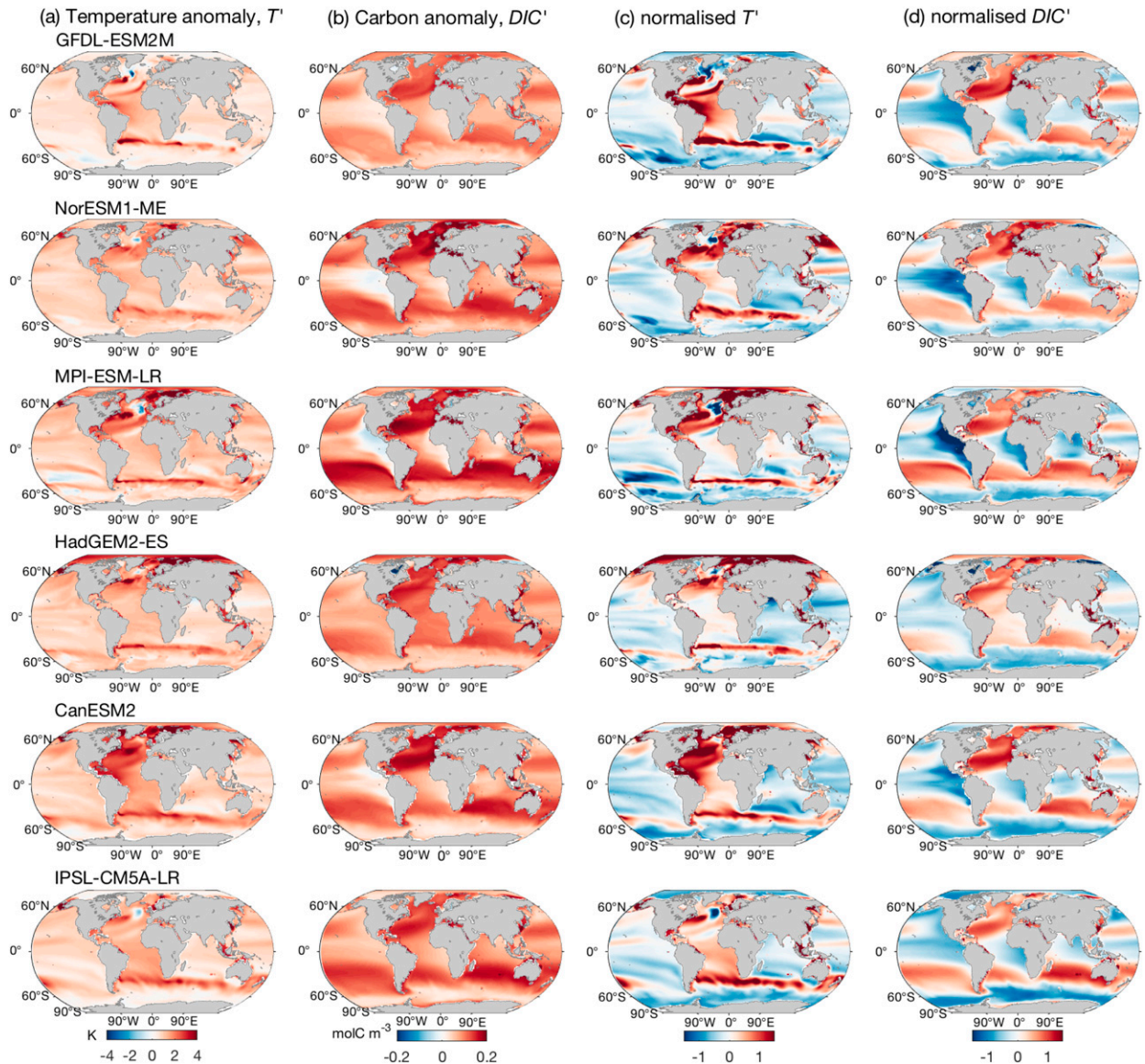


FIG. 1. Modeled change over the upper 1000 m for (a) upper ocean temperature anomaly $T'(x, y, t)$ (K), (b) dissolved inorganic carbon anomaly $DIC'(x, y, t)$ (mol C m^{-3}), and normalized anomalies for the (c) upper ocean temperature anomaly $T'(x, y, t)$, and (d) dissolved inorganic carbon anomaly $DIC'(x, y, t)$, for an annual 1% increase in CO_2 projections from GFDL-ESM2M, NorESM1-ME, MPI-ESM-LR, HadGEM2-ES, CanESM2M, and IPSL-CM5A-LR, averaged from years 100 to 140. The first three models have strong preindustrial Atlantic overturning, and the last two models have weak overturning. The normalization for a tracer anomaly c' is defined by $[c'(x, y, t) - \langle c'(x, y, t) \rangle] / \sigma_{c'}(t)$, where $\langle c'(x, y, t) \rangle$ is the global mean and $\sigma_{c'}(t)$ is the standard deviation based upon the spatial variations relative to the global mean at time t . The normalization reveals whether more tracer (in red) is locally stored than the global mean or whether less tracer (in blue) is locally stored than the global mean.

the global mean, while there is decrease in carbon storage relative to the global mean. In the northern high latitudes, there is a variability in the model response: in GFDL-ESM2M, a decrease in heat storage coincides with an increase in carbon storage relative to the global mean, while instead in CanESM2M there is an increase in heat and carbon storage.

A transport-based framework is next set out to understand the similarities and differences in the ocean heat and carbon storage, which is subsequently applied to a simplified climate

model and then to the tracer budgets for these CMIP5 models for the subpolar North Atlantic, the tropical Atlantic, and the entire Southern Ocean.

3. A transport-based framework for added and redistributed heat and carbon

The contrasts in the climate-driven changes in ocean storage of heat and carbon are now explored in terms of the added and

redistributed tracer. To understand their distinction, consider the evolution of a generic tracer $c(x, y, z, t)$ that satisfies a tracer equation

$$\frac{\partial c}{\partial t} + \mathbf{u} \cdot \nabla c = S, \quad (1)$$

where \mathbf{u} is the three-dimensional circulation and S is the net tracer source, including the effects of air–sea exchange and diffusive and mixing transfers. The tracer c is separated into a preindustrial value c_o at time t_o plus a time-dependent anomaly c' . The preindustrial tracer c_o is assumed to satisfy a steady tracer balance:

$$\mathbf{u}_o \cdot \nabla c_o = S_o. \quad (2)$$

The time-dependent tracer c' then satisfies a tracer equation from (1) and (2):

$$\frac{\partial c'}{\partial t} + (\mathbf{u}_o + \mathbf{u}') \cdot \nabla c' + \mathbf{u}' \cdot \nabla c_o = S', \quad (3)$$

where the tracer anomaly evolves in time through (i) the time-varying net source S' , (ii) the advection of the tracer anomaly $-(\mathbf{u}_o + \mathbf{u}') \cdot \nabla c'$, and (iii) the advection by the time-varying circulation of the preindustrial tracer distribution, $-\mathbf{u}' \cdot \nabla c_o$. Taking a time integral of (3) provides

$$c' = \underbrace{\int_{t_o}^t [S' - (\mathbf{u}_o + \mathbf{u}') \cdot \nabla c'] dt}_{\text{added tracer}} - \underbrace{\int_{t_o}^t \mathbf{u}' \cdot \nabla c_o dt}_{\text{redistributed tracer}}. \quad (4)$$

The tracer anomaly is then equivalent to (i) an added tracer, made up of the net source, including any effects of rising atmospheric CO_2 and climate-induced warming, plus the total advection of the tracer anomaly, and (ii) a redistributed tracer, accounting for the redistribution of the pre-existing tracer by the time-varying flow. The contribution of the redistributed tracer vanishes when (4) is integrated over a closed domain.

This transport-based separation in (4) is the same as how anthropogenic heat is separated into added heat and redistributed heat (Gregory et al. 2016). This transport-based separation differs in detail from carbon frameworks that separate the ocean carbon into anthropogenic carbon (Gruber et al. 1996; Hall et al. 2002; Sabine et al. 2004; Waugh et al. 2006) plus natural carbon (Bernardello et al. 2014; Thomas et al. 2018). While the increase in atmospheric CO_2 only affects anthropogenic carbon, climate-driven warming and time-varying changes in the circulation affect both the anthropogenic and natural carbon. In our framework, the redistributed carbon includes the transport effect of the time-varying circulations redistributing the preindustrial carbon and so is partly analogous to the natural carbon, but does not include other effects that alter the preformed and regenerated pools of natural carbon. The added carbon combines together all the other processes altering the ocean carbon, including how the net source varies with atmospheric CO_2 , solubility changes from warming, and the transport of added carbon by the total circulation.

Much of this invasion of excess heat and carbon into the ocean mimics the invasion of a passive tracer, where there is

uptake in the surface mixed layer and ventilation into the underlying thermocline. Thus, a passive invasion of heat and carbon might be expected to be broadly similar (Figs. 1a,b) (Sabine et al. 2004; Zanna et al. 2019; Bronselaer and Zanna 2020), although potentially differing in detail due to differences in their surface sources and interior cycling. However, the evolution of heat and carbon also includes a redistributed contribution involving the temporal change in the circulation advecting the preindustrial tracer distributions, $-\mathbf{u}' \cdot \nabla T_o$ and $-\mathbf{u}' \cdot \nabla \text{DIC}_o$, where T_o and DIC_o are the preindustrial temperature and dissolved inorganic carbon.

Following Winton et al. (2013), the ratio of the dynamic advection of the preindustrial tracer and the passive advection of the tracer anomaly is given by

$$\frac{\mathbf{u}' \cdot \nabla c_o}{\mathbf{u}_o \cdot \nabla c'} \sim \left(\frac{W'}{W_o} \right) \left(\frac{\Delta c_o}{\Delta c'} \right), \quad (5)$$

where W represents the typical magnitude of the vertical velocity and Δ represents a depth contrast in the tracer concentration. This scaling may also be interpreted as providing a nondimensional ratio for the redistributed tracer contribution divided by the added tracer contribution. There is a relatively large effect of the redistribution of tracer if the vertical gradients of the preindustrial tracer are comparable or larger than that of the tracer anomaly.

Winton et al. (2013) explained the different redistribution responses for heat and carbon in terms of this scaling (5) for how the magnitudes for the depth contrasts in the tracer anomaly and preindustrial tracer compare with each other. For our six Earth system models in Table 1, the ratio of the global-mean depth contrasts in the preindustrial and temporal change in temperature, $\Delta T_o / \Delta T'$, ranges from 7 to 14, while the ratio of the global-mean depth contrasts of the preindustrial and temporal change in dissolved inorganic carbon, $\Delta \text{DIC}_o / \Delta \text{DIC}'$, ranges from 1 to 2; here $\Delta c = c(z_1) - c(z_2)$ and represents the depth contrast in tracer concentration across the thermocline (taken between the upper 500 m and below 2500 m). The relative smallness of this ratio for carbon is a consequence of how the ocean holds a large background value of DIC through carbonate chemistry reactions, which only weakly vary with latitudinal temperature, salinity, and alkalinity changes over the surface ocean. The ratio of these vertical contrasts in temperature, $\Delta T_o / \Delta T'$, and carbon, $\Delta \text{DIC}_o / \Delta \text{DIC}'$, ranges in magnitude from 5 to 16 (Table 1), implying that the redistribution effect is much more important for the ocean gain in heat than for the gain in carbon.

The preindustrial tracer distributions have opposing gradients with surface subtropical waters being relatively warm and carbon depleted, while deep and high-latitude waters are relatively cool and carbon rich (Figs. A1c,d); these opposing gradients lead to opposing signs for the ratios of $\Delta T_o / \Delta T'$ and $\Delta \text{DIC}_o / \Delta \text{DIC}'$ in Table 1. Hence, a changing circulation is likely to lead to an opposing sign in the redistribution of heat and carbon due to the opposing sign in their preindustrial tracer gradients. This redistribution effect is next illustrated in a simplified climate model and then diagnosed for the set of CMIP5 models.

4. Evolution of added and redistributed heat and carbon in a simplified climate model

The contrasting heat and carbon responses to a changing overturning is now illustrated using a simplified climate model (Katavouta et al. 2019).

a. Model formulation

The simplified model consists of a slab atmosphere and five layers for the ocean (Fig. 2a), including a mixed layer overlying a thermocline layer in the low and middle latitudes, two upper layers for the southern and northern high latitudes, and a layer for the deep ocean.

The model is initially run to a steady state such that the net ocean carbon uptake at the preindustrial is zero. The model is forced by the equivalent emissions that correspond to an annual 1% increase in the atmospheric CO₂ for 98 years and then integrated toward equilibrium. The ocean carbon uptake due to air–sea flux of CO₂, denoted $\mathcal{F}_{\text{CO}_2}$, is distributed equally over the ocean surface area and is expressed as

$$\mathcal{F}_{\text{CO}_2} = \rho K_g \{K_o(t) \text{CO}_2(t) - [\text{CO}_2^s(t)]\}, \quad (6)$$

where ρ is a referenced density, K_g is a constant air–sea gas transfer coefficient, K_o is a time-dependent solubility varying with temperature, CO₂ is the mixing ratio of atmospheric CO₂, and [CO₂^s] is the concentration of the dissolved CO₂ at the ocean surface. The ocean carbon is held as dissolved inorganic carbon with its carbonate species solved for (Follows et al. 2006), so that the carbonate species alters with ocean acidity and temperature.

The increase in atmospheric CO₂ enhances the radiative forcing,

$$F(t) = a \ln[\text{CO}_2(t)/\text{CO}_2(t_o)], \quad (7)$$

where $a = 5.35 \text{ W m}^{-2}$ (Myhre et al. 1998) and the preindustrial CO₂ (t_o) is 280 ppm. This radiative forcing $F(t)$ drives a radiative response $R(t)$ plus a planetary heat uptake $N_p(t)$ (Gregory et al. 2004),

$$F(t) = R(t) + N_p(t) = \lambda T'_{\text{air}}(t) + N_p(t), \quad (8)$$

where the radiative response is assumed to depend on the surface air temperature anomaly $T'_{\text{air}}(t)$, multiplied by the climate feedback parameter λ ; here λ is taken to be constant and equal to $1 \text{ W m}^{-2} \text{ K}^{-1}$ for simplicity. The ocean heat uptake, N , is estimated as the planetary heat uptake minus the atmospheric heat uptake, $N(t) = N_p(t) - c[T'_s(t) - T'_{\text{air}}(t)]$, and is distributed equally over the surface ocean, where $c = 50 \text{ W m}^{-2} \text{ K}^{-1}$ is an air–sea heat transfer parameter and T'_s is the ocean surface temperature anomaly. For this model closure, the ocean heat uptake accounts for more than 95% of the planetary heat uptake.

The model solves for the thickness of the light water from a volumetric balance between the surface cooling conversion of light to dense waters in the North Atlantic, q_{NA} , the diapycnic transfer of dense to light waters, q_{m} , and the surface warming conversion of dense to light waters in the Southern Ocean, q_{SO} , (Gnanadesikan 1999; Marshall and Zanna 2014) such that

$$A \frac{dh(t)}{dt} = q_v(t) + q_{\text{SO}}(t) - q_{\text{NA}}(t), \quad (9)$$

where A is the surface ocean area in the low latitudes and h is the thickness of the combined mixed layer and thermocline in low latitudes.

Two different experiments are conducted using the simplified climate model, the meridional overturning is first kept constant and second allowed to evolve in time (Fig. 2b, solid line) and so alter the volumetric balance (9). The closure for the variable overturning assumes that the ocean heat uptake N , due to the extra radiative forcing from the rising atmospheric CO₂, acts to reduce the conversion of light to dense waters in the North Atlantic,

$$q'_{\text{NA}}(t) = -\frac{A N(t)}{\rho C_p \Delta T}, \quad (10)$$

where A is the surface ocean area in the low latitudes, $N(t)$ is the ocean heat uptake (W m^{-2}), ΔT is the temperature contrast between light and dense waters, ρ is density, and C_p is the specific heat capacity of seawater.

In each case, the model solves for the change in temperature and dissolved inorganic carbon based on the changes in heat and carbon transport, and the air–sea exchange of heat and carbon in the layered ocean model using (1). The added and redistributed temperature and dissolved inorganic carbon are diagnosed using (4). An explicit description of the model closure and tracer budget equations can be found in the appendix in Katavouta et al. (2019).

b. Heat and carbon response to changes in overturning

When the overturning circulation remains constant in time, there is a broadly similar distribution for the added heat and added carbon, both enhanced at low latitudes more than at high latitudes (Figs. 2c,d, dashed lines).

When the overturning circulation is allowed to evolve, there is also a dynamical redistribution of the preindustrial temperature and carbon distributions. The radiatively forced weakening in the overturning leads to a slight increase in the warming in low latitudes and a cooling in northern high latitudes (Fig. 2c, solid lines) and instead to a smaller contrast in the carbon held in the low and high latitudes (Fig. 2d, solid lines).

For this changing circulation, there is less heat storage in the northern high latitudes due to opposing effects of the added heat and redistributed heat. The added heat is positive (red line in Fig. 2e) from the combined effects of the atmospheric source and the transport of added heat to the high latitudes. The redistributed heat is instead negative (blue line in Fig. 2e) from the effect of the weakening overturning reducing the supply of warmer preindustrial low-latitude waters to the high latitudes. In contrast, there is an increase in carbon storage in the northern high latitudes from both the added carbon and the redistributed carbon reinforcing each other (Fig. 2f).

Hence, this idealized model illustrates how the added heat and carbon have a similar distribution, while a change in overturning leads to opposing signs for the redistributed heat and carbon.

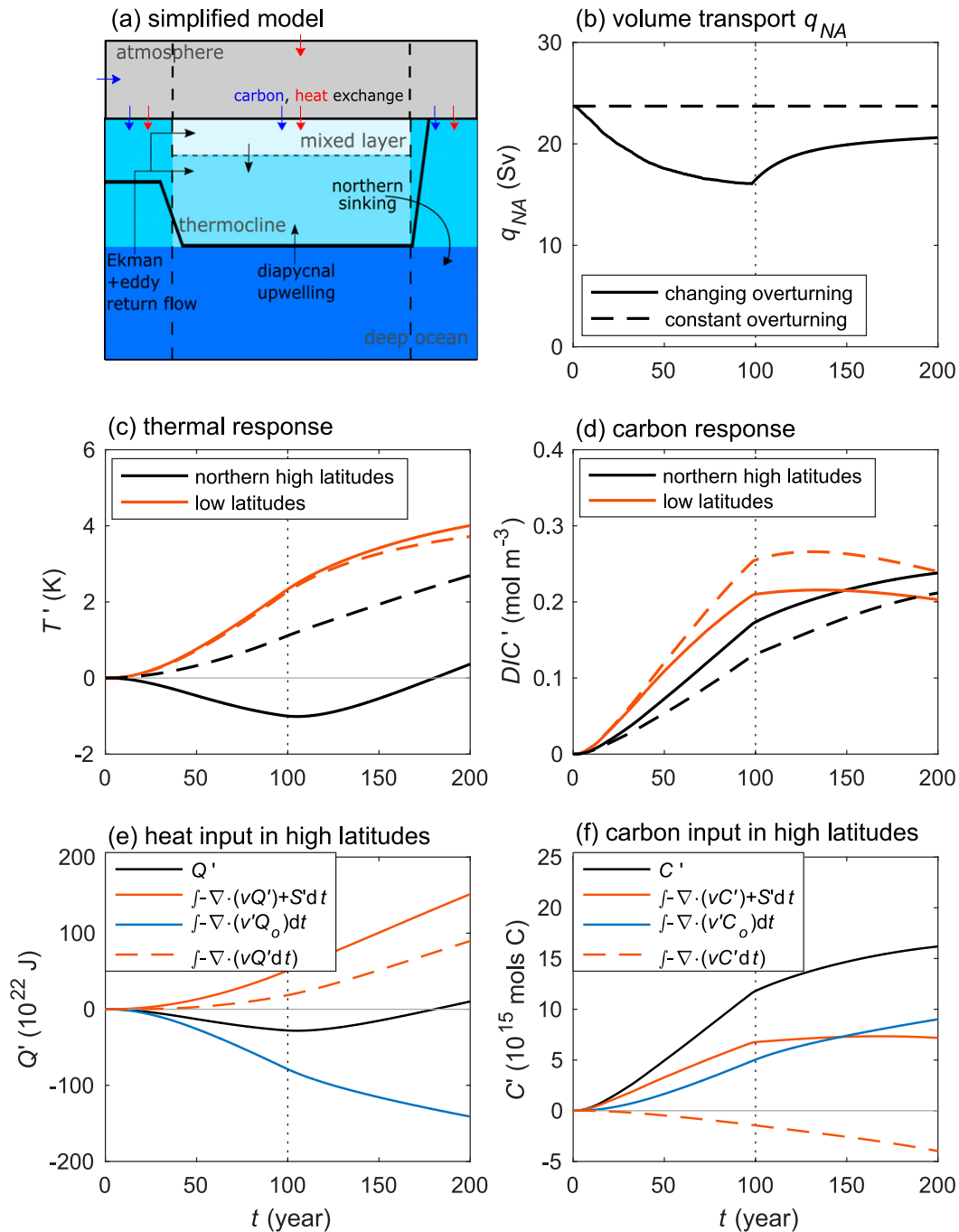


FIG. 2. (a) A simplified climate model forced by a carbon emission (blue arrow on the side) and experiencing additional radiative forcing (red arrow at top). The model consists of a slab atmosphere and five boxes for the ocean. (b) The evolution of the meridional overturning circulation involving the transformation of light to dense water in the northern high latitudes, q_{NA} (Sv), which decreases in time (solid line) during carbon emissions (up to year 98; dotted line) or is artificially assumed to be constant in time (dashed line). (c) Temperature change in the upper ocean in the northern high latitudes (black line) and low latitudes (red line), T' (K). (d) Carbon change in the upper ocean in the northern high latitudes (black line) and low latitudes (red line), DIC' (mol m^{-3}). (e) Heat gain Q' in the upper ocean in the northern high latitudes (10^{22} J). (f) Carbon gain C' in the upper ocean in the northern high latitudes (10^{15} mol C). The heat and carbon gain are separated into the added heat and carbon (red line) and the redistributed heat and carbon (blue line). The added tracer (red line) is defined by the time integral of the convergence of the transport of time-varying tracer plus the net source of the time-varying tracer (dashed red line). The redistributed tracer (blue line) is defined by the time integral of the time-varying transport of the preindustrial tracer.

TABLE 2. Overturning and residual circulation metrics for the six CMIP5 Earth system models forced by an annual 1% rise in atmospheric CO₂: preindustrial overturning Ψ_o and the overturning anomaly at year 100 Ψ' . The values are evaluated as the overturning maximum over the upper 2000 m and its subsequent largest change either for the North Atlantic or between 60° and 40°S for the Southern Ocean.

Earth system model	North Atlantic		Southern Ocean	
	Ψ_o (Sv)	Ψ' (Sv)	Ψ_o (Sv)	Ψ' (Sv)
GFDL-ESM2M	25.5	−10.2	20.8	9.6
NorESM1-ME	33.0	−10.2	27.0	7.7
MPI-ESM-LR	23.9	−12.5	40.0	19.8
HadGEM2-ES	15.5	−6.0	42.2	6.4
CanESM2M	14.8	−3.1	33.7	14.3
IPSL-CM5A-LR	12.8	−7.4	34.6	10.0

5. Climate-driven changes in ocean heat and carbon storage for a set of Earth system models

The evolution of the ocean heat and carbon storage is now examined in terms of their added and redistributed components for the six CMIP5 Earth system models.

a. Changes in meridional overturning and residual circulation

There are contrasting changes in the circulation with a projected weakening of the Atlantic meridional overturning and a strengthening in the Southern Ocean residual circulation. The preindustrial Atlantic meridional overturning reaches more than 20 Sv (1 Sv $\equiv 10^6 \text{ m}^3 \text{ s}^{-1}$) for three of the models (GFDL-ESM2M, NorESM1-ME, and MPI-ESM-LR), but only reaches from 13 to 16 Sv for the three other models (Table 2, Fig. 3a). The overturning weakens for all the models by year 100 with a larger weakening for those models with a stronger preindustrial overturning (Fig. 3b).

In comparison, the preindustrial residual circulation in the Southern Ocean between 40° and 60°S ranges from 21 to 42 Sv (Table 2, Fig. 3a). The residual circulation strengthens from the preindustrial to year 100 for all the models with an amount ranging from 6 to 20 Sv (Fig. 3b).

These overturning circulations are important in advecting the added heat and carbon, as well as redistributing the preindustrial heat and carbon.

b. Transport of added and redistributed heat and carbon

The preindustrial overturning acts in a similar manner for added heat and carbon, transporting added tracer northward over the Atlantic sector (Figs. 4a,b), and so providing a northern accumulation of heat and carbon. There is an elevated gain in heat and carbon over the upper ocean, usually coinciding with the thicker thermoclines of the subtropics, centered at 25°S and 25°N. There are intermodel differences in the temporal change in temperature, such as with a marked cooling north of 50°N versus a warming at 40°N for GFDL-ESM2M (Fig. 4a). The temporal change in carbon distributions is more similar to each other across these models (Fig. 4b).

The change in the overturning acts to redistribute the preindustrial temperature and carbon. The weakening in the overturning decreases the northward transport of surface warm waters and so acts to reduce the heat supply to northern high latitudes (Fig. 4c). The weakening in the overturning acts to reduce the northward transport of surface waters with relatively low carbon content (Fig. 4d) and so acts to enhance the accumulation of carbon in the northern high latitudes. The extent of these effects differs between the models according to both their weakening in overturning and reconstructions of preindustrial carbon; for example, there is a relatively low preindustrial carbon content in the tropics for HadGEM2-ES.

Hence, the weakening in the overturning acts in an opposing manner for heat and carbon, reducing the redistribution of heat to the northern high latitudes, but enhancing the redistribution of carbon.

c. Tracer budgets for added and redistributed heat and carbon

Tracer budgets for the temporal change in heat and carbon are next examined for three different regimes: the subpolar North Atlantic, the tropics, and the Southern Ocean. A flux form of the heat and carbon budgets are time integrated, combining (4) with the continuity of volume, and are interpreted in terms of their added and redistributed tracer:

$$c' = \underbrace{\int_{t_o}^t [S' - \nabla \cdot (\mathbf{u}c')] dt}_{\text{added tracer}} - \underbrace{\int_{t_o}^t \nabla \cdot (\mathbf{u}'c_o) dt}_{\text{redistributed tracer}}. \quad (11)$$

The time-varying heat and carbon budgets are further integrated over a control volume that extends in the vertical from the surface to either a depth of 300 or 1000 m, and horizontally within latitude bands, either running coast to coast or around the globe. The domains for each model are chosen to be indicative of similar dynamical regimes, rather than cover exactly the same geographical region, so differ according to their preindustrial tracer distributions and changes in the overturning.

The tracer transports through the meridional sides and bottom boundary of the control volume are calculated from the area integrals of the product of the velocity and the tracer concentration, where the velocity includes the effect of the eddy transport closure. The meridional tracer transport is calculated as a zonal and vertical integral of the product of the meridional velocity and the tracer. The overturning component is the vertical integral of the product of the zonally averaged tracer and the zonal integral of the meridional volume transport. The gyre component is the difference between the total and the overturning transports.

The volume-averaged tracer anomaly c' is diagnosed from the tracer distributions and the redistributed tracer from the convergence of the transport of the preindustrial tracer. The added tracer is estimated from (11) and from the estimate of the transport of tracer anomaly, the net source S' is diagnosed, which then represents the effect of air–sea exchange and mixing, as well as any residual errors in our approach. The tracer budgets are assessed every year from the start to the end of the integration using the available annual-mean model

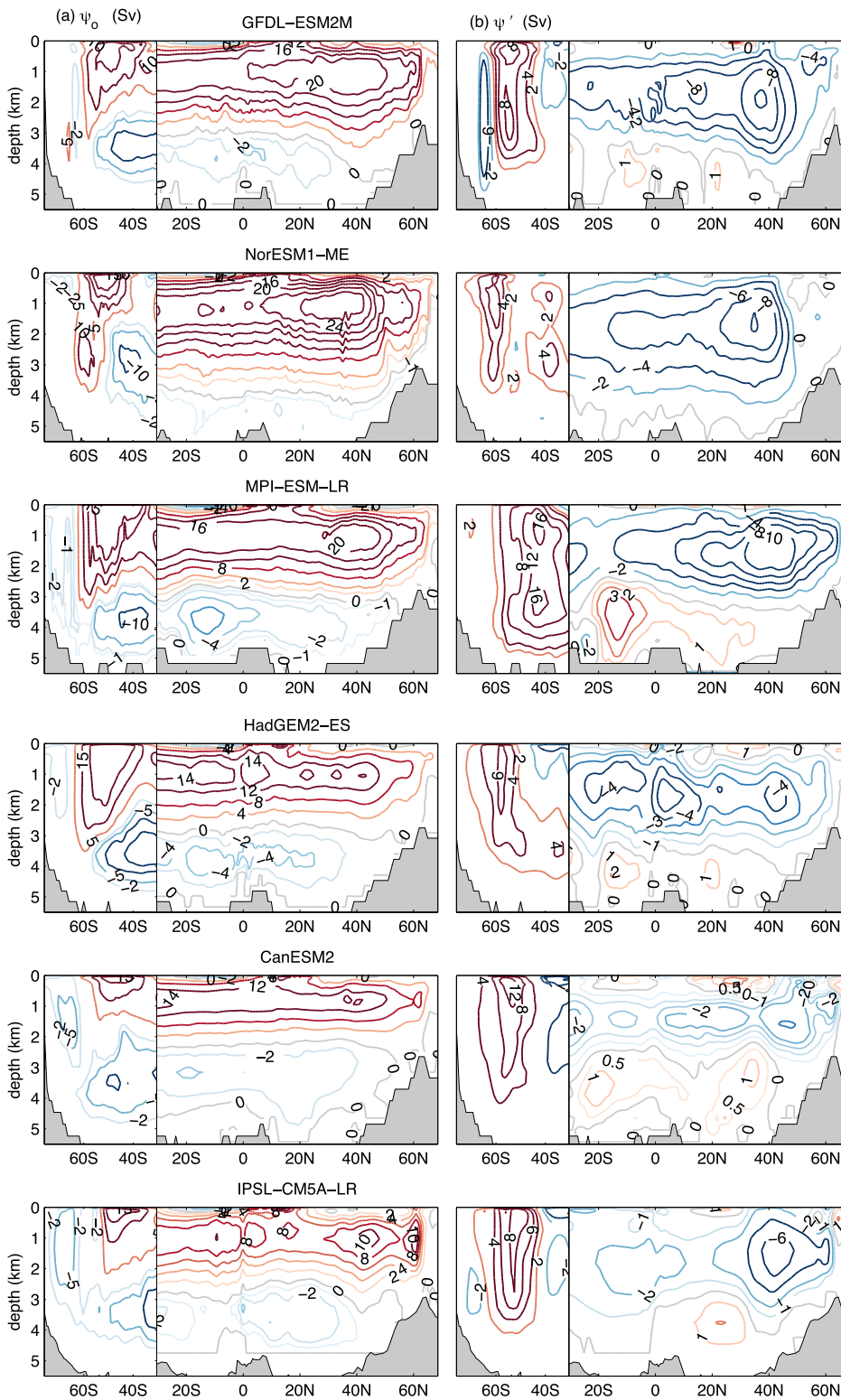


FIG. 3. The meridional overturning streamfunction Ψ (Sv) for the Atlantic basin and the residual overturning for the entire Southern Ocean (domains separated by the thin line) for GFDL-ESM2M, NorESM1-ME, MPI-ESM-LR, HadGEM2-ES, CanESM2M, and IPSL-CM5A-LR for (a) the preindustrial Ψ_0 , and (b) the perturbation at year 100, Ψ' . The residual overturning includes the Eulerian-mean overturning and the parameterized eddy-driven circulation.

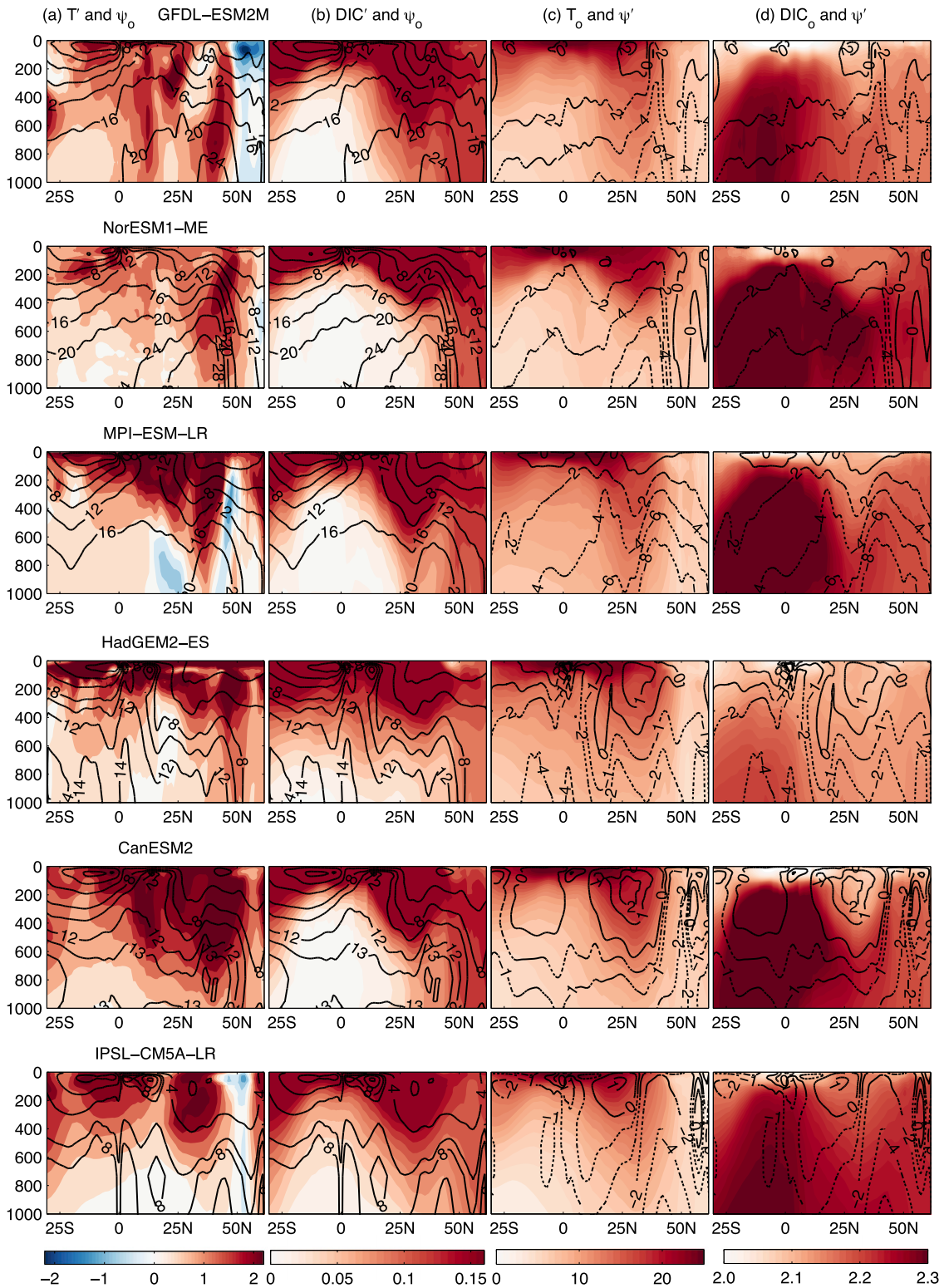


FIG. 4. Meridional section in the Atlantic over the upper 1 km for the six Earth system models: (a) the temporal change in temperature T' (K) and preindustrial overturning streamfunction ψ_0 (Sv, contours); (b) the temporal change in dissolved inorganic carbon DIC' (mol m^{-3}) and preindustrial overturning ψ_0 ; (c) preindustrial temperature T_0 and temporal change in overturning ψ' ; and (d) preindustrial carbon DIC_0 and temporal change in overturning ψ' . The preindustrial values are taken from the initial state and the temporal changes in the tracer and streamfunction for year 100.

output of the full velocity, potential temperature, and the dissolved inorganic carbon.

d. Tracer budgets for the subpolar North Atlantic

The subpolar North Atlantic varies from being a region of relatively enhanced to reduced heat storage relative to the global mean, while always being a site of enhanced carbon storage for the models (Figs. 5a,b, maps). To understand these differing responses, tracer budgets are evaluated using (11) for a volume integral over the subpolar North Atlantic covering the upper 1000 m of the middle to high latitudes, extending from the northern flank of the subtropical gyre and over much of the subpolar gyre (dashed lines in maps in Fig. 5).

1) ADDED AND REDISTRIBUTED HEAT

The subpolar heat budget reveals positive added heat versus negative redistributed heat across five models (Fig. 5a, red and blue lines). The exception is IPSL-CM5A-LR, one of the models with a weaker overturning, which shows weaker signals with opposing signs for the first 70 years, but after then the same signed response as the other models.

The added heat is achieved in different ways. For three models, the added heat is supplied by the net source (Fig. 5a, red dotted lines), while for the other three models the added heat is instead carried into the domain by the preindustrial circulation (Fig. 5a, red dashed lines).

The redistributed heat is always negative for five of the models and eventually negative for IPSL-CM5A-LR after 70 years (Fig. 5a, blue lines). A weakening in the combined effects of the gyre and overturning circulations leads to less heat being transported into the subpolar domain (as illustrated in Fig. 4c for a weaker overturning). This weakening in heat supply is most pronounced for those models that have a strong preindustrial overturning (Fig. 3).

2) ADDED AND REDISTRIBUTED CARBON

The subpolar carbon budget reveals positive added and redistributed carbon for all the models (Fig. 5b, red and blue lines). The added carbon is dominated by the supply from the net source in five of the models (Fig. 5b, red dotted line), while instead for MPI-ESM-LR the supply is from the convergence of the passive transport of added carbon (Fig. 5b, red dashed line).

The supply of carbon from the dynamic redistribution is positive in all the models (Fig. 5b, blue lines), associated with a weaker influx of relatively carbon-poor waters from low latitudes from a weaker overturning and gyre circulations. This dynamic redistribution is largest in magnitude when there is a strong weakening in the overturning, such as for GFDL-ESM2M.

In summary, the added and redistributed carbon contributions reinforce each other for all the models, leading to the subpolar North Atlantic consistently being a region of enhanced carbon storage. In contrast, the added and redistributed heat contributions nearly always oppose each other, so that the subpolar North Atlantic varies between being a region of enhanced and reduced heat storage.

e. Tracer budgets for the tropical Atlantic

Over the upper tropical Atlantic, there is a relatively enhanced heat storage versus relatively reduced carbon storage for five out of six of the models relative to their global mean (Figs. 6a,b, maps). The exception is HadGEM2-ES where the heat storage is close to the global mean and the carbon storage is greater than the global mean. To reveal why there are these contrasting heat and carbon responses, tracer budgets (11) are evaluated over the upper 300 m for a tropical region (dashed lines in maps in Fig. 6).

1) ADDED AND REDISTRIBUTED HEAT

The tropical heat budget reveals an eventual loss in added heat for five out of six of the models, and an eventual gain in redistributed heat for all six models (Fig. 6a, red and blue lines). The exception is IPSL-CM5A-LR where there is a weak gain in both added heat and redistributed heat.

The added heat involves a competition between the effects of the net source and the convergence in the transport of added heat. For five of the models, the net source of added heat is positive for these models (Fig. 6a, red dotted lines), while the added heat is eventually negative through the upwelling providing depleted added heat to the surface layer (Fig. 6a, red dashed lines). Instead for the exception HadGEM2-ES, there is a convergence of added heat and the net source provides a loss of added heat, consistent with downward mixing of added heat out of the surface layer and there being a strong vertical gradient in added temperature.

The redistributed heat is eventually positive for all of the models due to a weakening in the upwelling leading to a reduced supply of cooler waters to the surface layer (Fig. 6a, blue lines). The timing of this gain in redistributed heat varies in the models from between the start and 60 years into the integration.

2) ADDED AND REDISTRIBUTED CARBON

The regional carbon budget in the tropical Atlantic reveals a positive contribution from the added carbon for all six models and a negative contribution from the redistributed carbon for five of these models (Fig. 6b, red and blue lines).

The added carbon is positive due to a net source of added carbon for all the models (Fig. 6b, red dotted lines). For five of the models, the added carbon is also affected by a divergence in the transport of added carbon with added carbon being transported out of this tropical upper layer. Instead for HadGEM2-ES there is a convergence of added carbon (Fig. 6b, red dashed lines).

The redistributed carbon is negative over the tropical Atlantic for nearly all the models due to a weakening in the upwelling of carbon-rich deep waters to the surface layer (Fig. 6b, blue lines). The redistributed carbon is instead close to zero for HadGEM2-ES, which is due to an absence of a strong, vertical gradient in preindustrial carbon in the tropics (Fig. 4d).

In summary, the relatively enhanced gain of heat and relatively reduced gain of carbon in the tropical Atlantic corresponds to differences in their net sources and the opposing signs of the dynamical redistribution of heat and carbon, where a weaker upwelling provides a reduced supply of cold, carbon-rich waters to the surface layer.

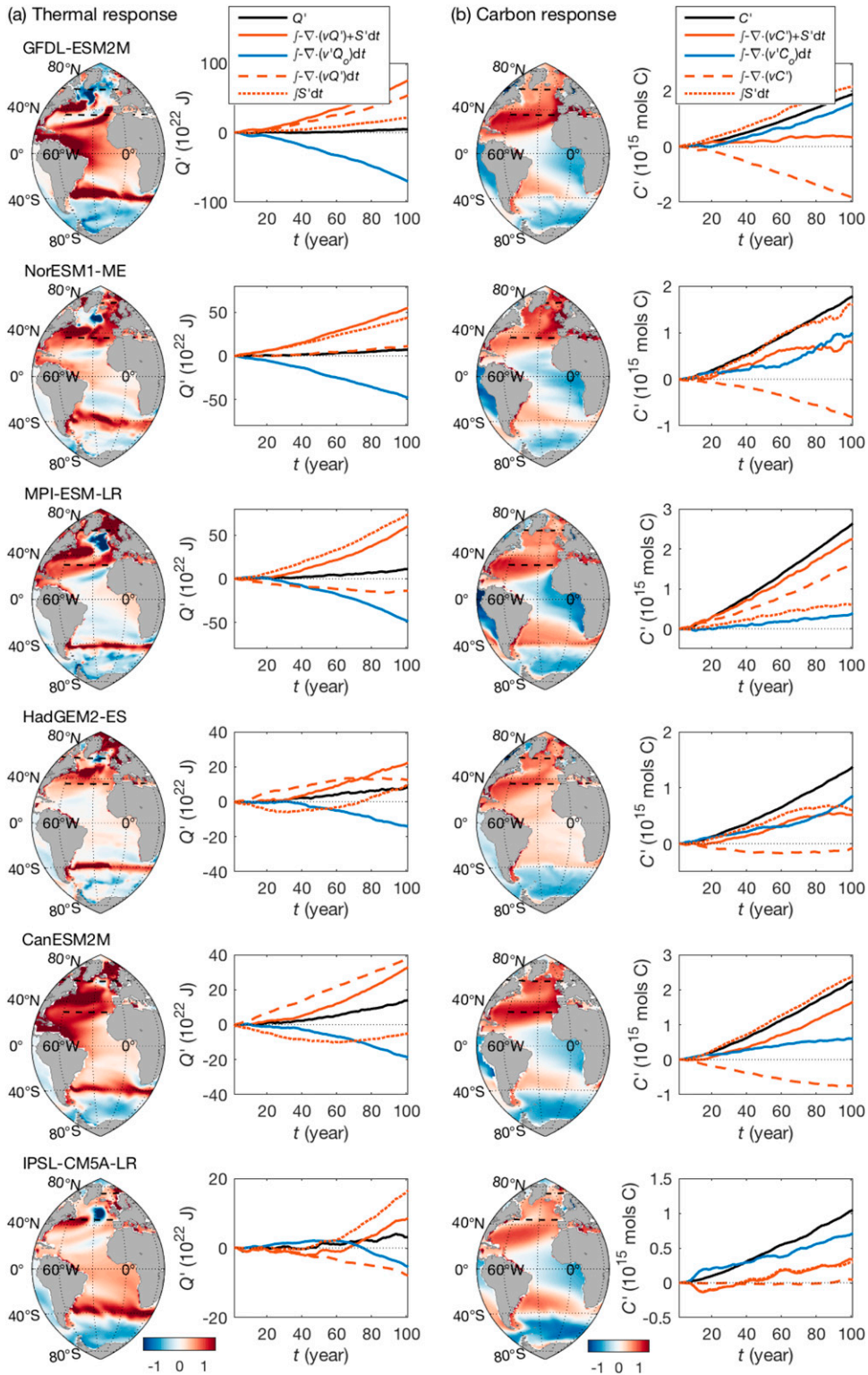


FIG. 5. Normalized anomalies for temporal changes in (a) heat and (b) carbon over the upper 1000 m for the subpolar North Atlantic: GFDL-ESM2M (35°–60°N), NorESM1-ME (35°–70°N), MPI-ESM-LR (31°–65°N), HadGEM2-ES (35°–60°N), CanESM2M (30°–60°N), and IPSL-CM5A-LR (45°–72°N). In the tracer budget for the subpolar domain (dashed black lines), the tracer anomaly (black line) is made up of the added tracer (red line) and redistributed tracer (blue line). The added tracer includes contributions from the time integral of the net source (red dotted line) and the advection of added tracer (dashed red line).

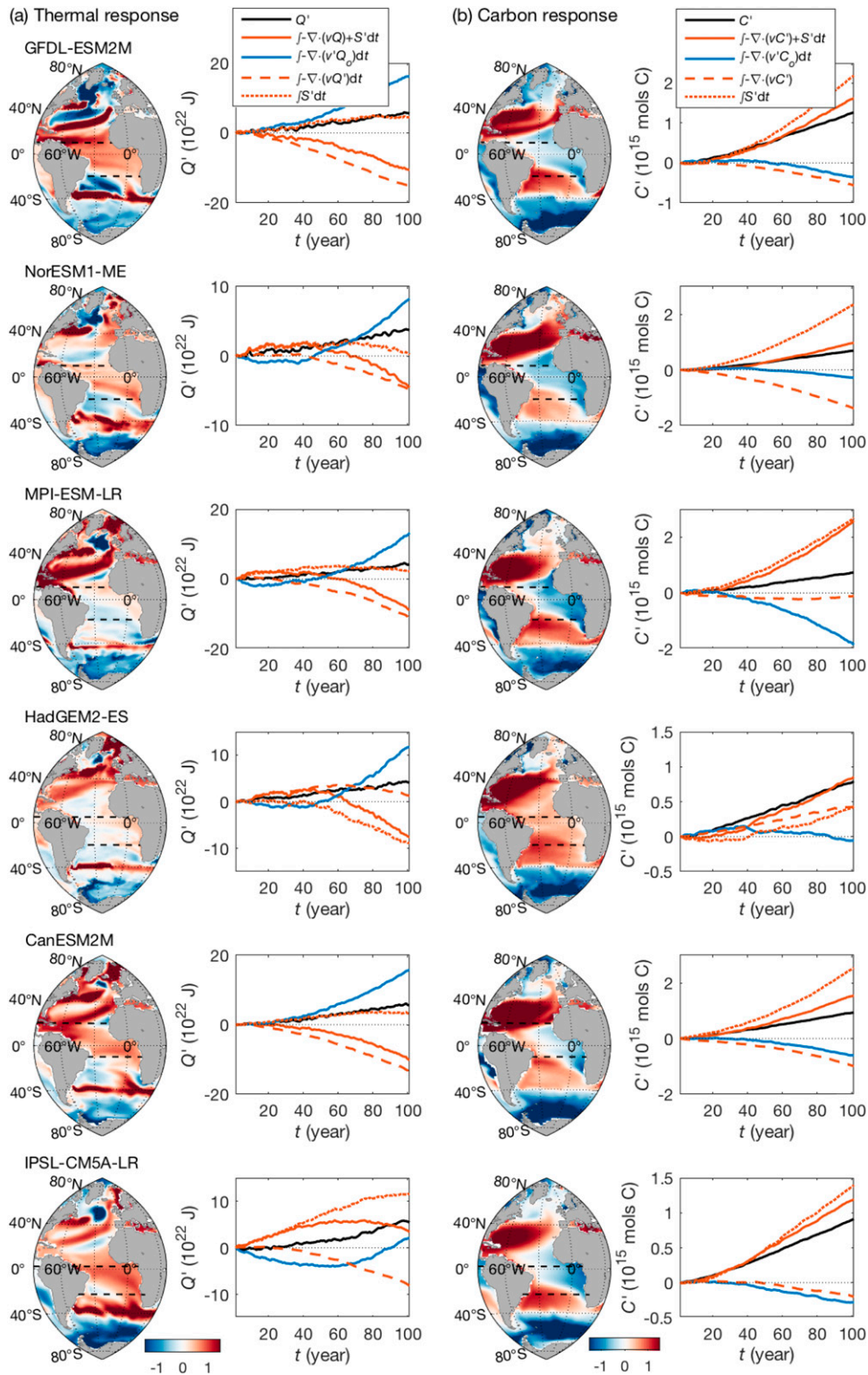


FIG. 6. Normalized anomalies for temporal change in (a) heat and (b) carbon over the upper 300 m for the tropical Atlantic: GFDL-ESM2M (20°S–10°N), NorESM1-ME (20°S–10°N), MPI-ESM-LR (18°S–11°N), HadGEM2-ES (20°S–5°N), CanESM2M (10°S–20°N), and IPSL-CM5A-LR (25°S–2°N). In the tracer budget for the tropical domain (dashed black lines), the tracer anomaly (black line) is made up of the added tracer (red line) and redistributed tracer (blue line). The added tracer includes contributions from the time integral of the net source (red dotted line) and the advection of added tracer (dashed red line).

f. Tracer budgets for the Southern Ocean

In the Southern Ocean, the climate-driven increases in heat and carbon storage over the upper 1000 m are enhanced between the latitudes of 40° and 60°S, and then become depleted south of 60°S relative to their global mean (Figs. 7a,b, maps). The enhanced heat storage occurs over a narrow, spiraling band, extending from the South Atlantic at 40°S to south of South Africa and Australia and sometimes extending farther to the eastern Pacific (Fig. 7a). In contrast, the enhanced carbon storage is more extensive over much of the Southern Ocean (Fig. 7b).

To understand how these responses are controlled, tracer budgets (11) are diagnosed over the upper 1000 m for the entire Southern Ocean, zonally integrated from Antarctica to typically 40°S.

1) ADDED AND REDISTRIBUTED HEAT

The regional heat budget for the Southern Ocean reveals an overall positive contribution from the added heat and a negative contribution from the redistributed heat for four models (Fig. 7a, red solid and blue lines). The two exceptions, CanESM2M and IPSL-CM5A-LR, reveal the same response as the other models after 70 years.

The added heat involves a positive contribution from the net source (Fig. 7a, red dotted lines), which is augmented by the supply of added heat by the preindustrial circulation (Fig. 7a, red dashed line). This added heat supply is achieved by the preindustrial gyre circulation providing a southward transport of added heat into the domain (Fig. 8a, red dotted line). In contrast, the preindustrial meridional overturning circulation provides a northward transport of added heat out of the domain and to northern latitudes (Fig. 8a, red dashed line), consistent with previous studies (Marshall et al. 2015; Armour et al. 2016).

The redistributed heat is always negative over the Southern Ocean for four models, as well as eventually becomes negative for IPSL-CM5A-LR and CanESM2M after 50 to 70 years (Fig. 7a, blue line). This response is due to the change in the gyre circulation and the strengthening in the overturning circulation leading to an increase in the northward transport of heat out of the domain to northern latitudes (Fig. 8a, blue dotted and dashed lines).

2) ADDED AND REDISTRIBUTED CARBON

The regional carbon budget for the Southern Ocean reveals positive contributions for the added carbon for all the models and for the redistributed carbon for five of the models (Fig. 7b, red solid and blue lines) with a very small increase for IPSL-CM5A-LR.

The added carbon is positive from the net source (Fig. 7b, red dotted lines), which is opposed by the passive loss in added carbon from a northward transport of added carbon by the preindustrial circulation out of the domain (Fig. 7b, red dashed line). This loss of added carbon is achieved mainly by the meridional overturning and augmented by the gyre circulation (Fig. 8b, red dashed and dotted lines).

The redistributed carbon is weakly positive for five of the models (Fig. 7b) but involves a range of responses. There are

reinforcing contributions from temporal changes in the gyre circulation and the strengthening in the overturning circulation for three of the models (GFDL-ESM2M, HadGEM2-ES, and CanESM2M), while there are opposing contributions for the other three models with a slight dominance of the overturning (Fig. 8b, blue dashed and dotted lines). For IPSL-CM5A-LR, there is a lack of a signal of redistributed carbon due to the opposing contributions from the overturning and gyre circulations.

In summary, the Southern Ocean takes up both climate-driven changes in heat and carbon, as previously documented (Frölicher et al. 2015). The heat storage involves a competition between the opposing effects of added and redistributed heat, while the carbon storage involves the added and redistributed carbon reinforcing each other. Consequently, the patterns of heat storage reveal more horizontal structure than seen in the patterns of carbon storage.

6. Discussion

The ocean plays a crucial role in sequestering the extra heat and carbon supplied to the climate system. The ocean gain in heat and carbon might plausibly be viewed as occurring in a similar manner, with both uptakes involving an atmospheric source, transfer into a surface mixed layer, and subsequent transfer following ventilation pathways into the thermocline and deep ocean. The extent to which the ocean storage of heat and of carbon resemble each other is investigated here using a simplified climate model and diagnostics for a suite of six CMIP5 Earth system model projections following an idealized 1% annual rise in atmospheric CO₂ over 100 years. Diagnostics of the CMIP5 models reveal consistently enhanced storage of heat and carbon in the subtropics and relatively reduced storage in the high latitudes of the Southern Ocean. However, there are intermodel differences in the gain in heat and carbon storage, sometimes including opposing responses in the subpolar North Atlantic and the tropical Atlantic relative to the global-mean response.

The regional similarities and differences in the ocean heat and carbon storage are understood here using a transport-based framework, where regional changes in tracer storage are separated into contributions from the added tracer and redistributed tracer. The added tracer includes the effect of a net source and the effect of the preindustrial and time-varying circulation in transporting added tracer. The redistributed tracer includes the effect of the time-varying circulation in redistributing the preindustrial tracer distributions. The climate-driven changes in heat storage have previously been understood in this manner (Banks and Gregory 2006; Xie and Vallis 2012; Gregory et al. 2016; Zanna et al. 2019), but this approach is not usually applied for accompanying changes in carbon storage.

For the carbon community, the carbon response is usually viewed in terms of anthropogenic and natural carbon responses. The natural carbon alters through changes in preformed and regenerated pools of carbon, including variations in the solubility of CO₂ and changes in the circulation redistributing natural carbon (Bernardello et al. 2014; Thomas et al. 2018). The uptake of anthropogenic carbon from the atmosphere is estimated from how a quasi-conserved carbon tracer spreads into the interior (Gruber et al. 1996; Sabine et al. 2004;

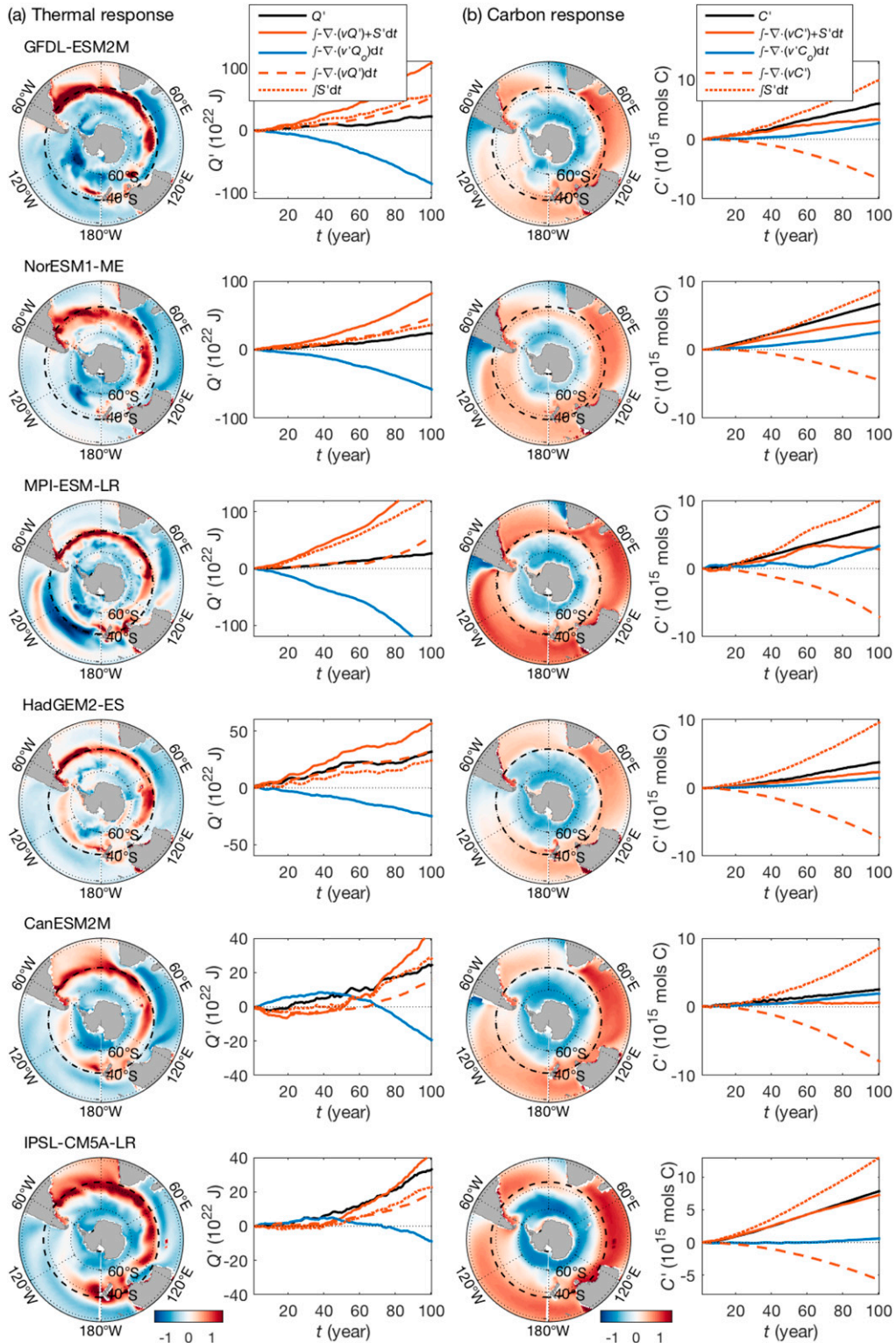


FIG. 7. The normalized anomalies for the temporal change in (a) heat and (b) carbon over the upper 1000 m for the Southern Ocean for GFDL-ESM2M (80° – 37° S), NorESM1-ME (79° – 37° S), MPI-ESM-LR (77° – 41° S), HadGEM2-ES (80° – 40° S), CanESM2M (80° – 41° S), and IPSL-CM5A-LR (78° – 36° S). In the tracer budget for the domain (dashed black lines), the tracer anomaly (black line) is made up of the added tracer (red line) and redistributed tracer (blue line). The added tracer includes contributions from the time integral of the net source (dotted red line) and the advection of added tracer (dashed red line).

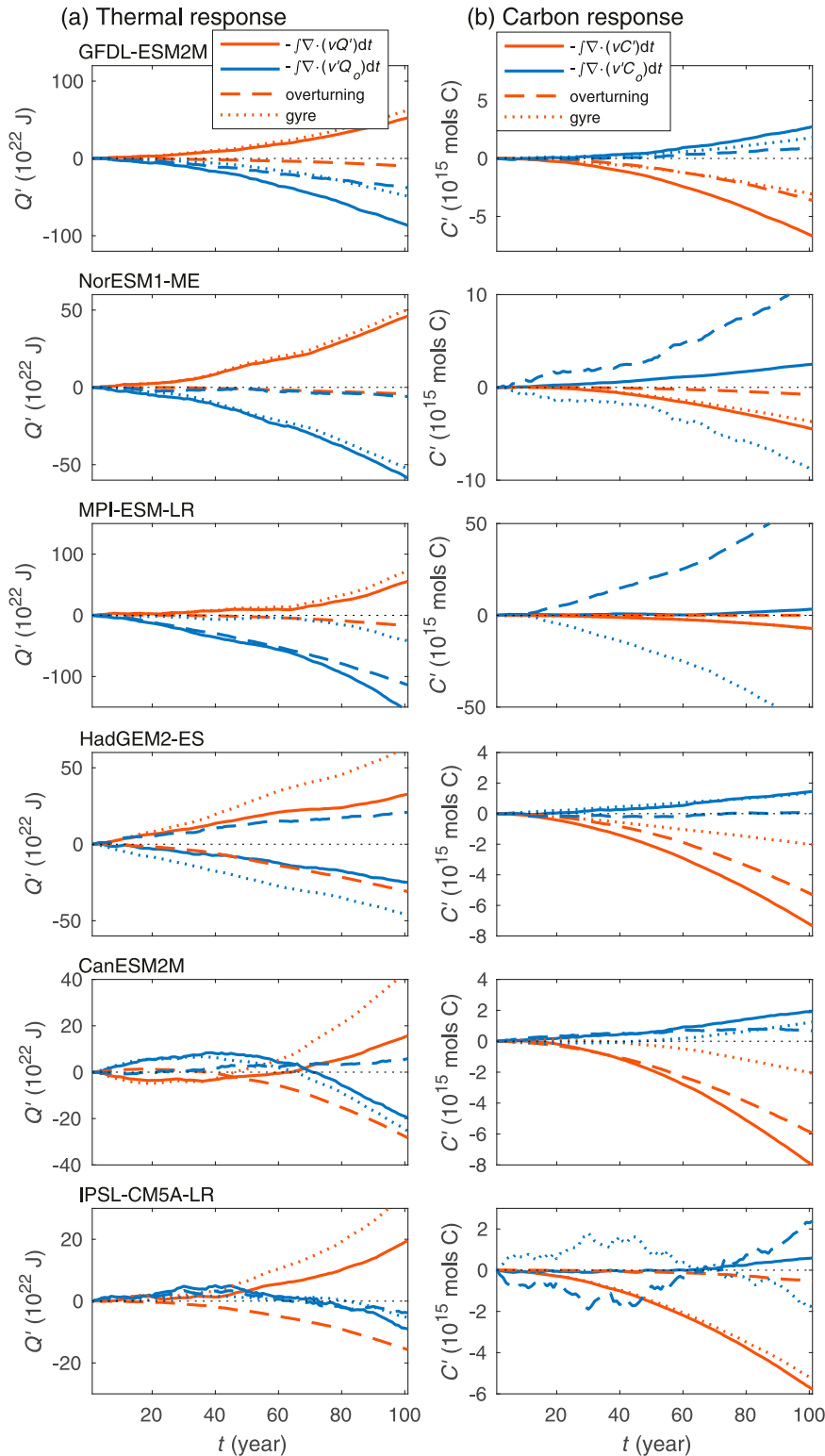


FIG. 8. The time-integrated convergence of the transport of (a) heat and (b) carbon over the upper 1000 m for the Southern Ocean for GFDL-ESM2M (80°–37°S), NorESM1-ME (79°–37°S), MPI-ESM-LR (77°–41°S), HadGEM2-ES (80°–40°S), CanESM2M (80°–41°S), and IPSL-CM5A-LR (78°–36°S). In the transport budget, the supply from the circulation acting on the temporal change in tracer (red line, same as the dashed red line in Fig. 7) and the dynamic supply from the time-varying circulation redistributing the preindustrial tracer (blue line) are each separated into overturning (dashed line) and gyre (dotted line) contributions.

Clement and Gruber 2018) or from the spreading of passive tracers, such as CFCs, usually assuming an unchanging circulation (Vaugh et al. 2006; Khatiwala et al. 2009; DeVries 2014). The Atlantic overturning is viewed as transporting natural carbon southward (Resplandy et al. 2018) and anthropogenic carbon northward (DeVries 2014), and changes in the circulation can alter both the anthropogenic and natural carbon (DeVries et al. 2017).

The definitions of anthropogenic carbon and natural carbon are similar, but not the same as our transport-based definitions of added and redistributed carbon. In our framework, the redistributed carbon includes the transport effect of the time-varying circulations redistributing the preindustrial carbon and so is partly analogous to the natural carbon, but does not include other effects that alter the preformed and regenerated pools of natural carbon. Over the global ocean, the changes in redistributed carbon integrate to zero, while changes in natural carbon need not integrate to zero. The added carbon combines together all the other processes altering the ocean carbon, including how the net source varies with atmospheric CO₂, solubility changes from warming, and the transport of added carbon by the total circulation. Over the global ocean, the volume integral of the added carbon is the same as the volume integral of the sum of the anthropogenic and natural carbon.

Our simplified climate model reveals that there is a broadly similar addition of heat and carbon when there is a fixed overturning, but there are opposite-signed contributions in the redistribution of heat and carbon when there is a change in the overturning. There is a broadly similar response in the diagnostics of the CMIP5 models for the subpolar North Atlantic, the tropical Atlantic, and the Southern Ocean. In the subpolar North Atlantic, there is consistently more carbon storage with both a supply of carbon from added and redistributed carbon, while there is a variable heat storage with the added heat opposed by a negative redistributed heat; the redistribution is associated with a weakening in the overturning, supplying less heat and a lower amount of carbon-depleted waters. In the tropical Atlantic, there is a relatively enhanced storage of heat and relatively reduced storage of carbon, which is due to a weaker upwelling providing a positive redistributed heat and negative redistributed carbon from the reduced supply of cold, carbon-rich waters to the surface layer. In the Southern Ocean, the heat storage again involves a competition between the opposing effects of added and redistributed heat, while the carbon storage involves the added and redistributed carbon reinforcing each other. Consequently, the patterns of heat storage reveal more horizontal structure than seen in the patterns of carbon storage.

In all of these regions, the added heat and carbon usually have a similar sign due to the dominance of the net source to the surface layer. The redistributed heat and carbon contributions are instead always opposing in sign due to their opposing preindustrial temperature and carbon gradients. Consequently, there are regions where the patterns of climate-driven changes in heat and carbon are similar to each other when the added contributions dominate. In contrast, there are regions where the patterns of climate-driven changes in heat and carbon relative to the global-mean responses are opposite to each other when the redistributed contributions

dominate. The redistribution effect is more prominent for temperature than carbon (Winton et al. 2013) due to the relatively large contrast in preindustrial temperature compared with preindustrial carbon. Hence, there is a larger intermodel spread in the warming response and a more uniform carbon response.

For the projected weakening in the Atlantic overturning and the strengthening of the Southern Ocean residual circulation, there are differing responses in the high latitudes with the heat anomalies of a variable sign and the carbon anomalies of a consistent positive sign. This response is due to the redistributed heat usually being negative and the redistributed carbon being positive for these circulation changes. Hence, the added and redistributed heat usually oppose each other at high latitudes, while the added and redistributed carbon anomalies reinforce each other at high latitudes.

The global diagnostics of ocean heat and carbon storage are dominated by the addition of heat and carbon, as exploited in a recent study of Bronselaer and Zanna (2020) that uses the distribution of carbon storage to constrain estimates of added heat. This extrapolation is appropriate when the redistribution of carbon is relatively small, but we find on time scales of 100 years the redistribution of carbon becomes important over some basins. Our study is consistent with variability in the global model diagnostics of heat and carbon content being anticorrelated with each other on decadal to centennial time scales (Thomas et al. 2018).

This study of how thermal and carbon anomalies coincide has implications for likelihood of different marine hazards coinciding, including whether warming events coincide with acidification events (Gruber 2011). For example, marine heat waves have been reported lasting between days to months, where an extensive region experiences elevated surface temperature (Frölicher et al. 2018). A shift to a warmer climate is expected to lead to many more marine heat waves compared with the number of land-based heat waves due to the relatively narrow sea surface temperature distribution (Frölicher and Laufkötter 2018). If the climate-driven changes in surface temperature and surface carbon are mainly a result of added heat and added carbon, then more reinforcing thermal and acidifying hazards are to be expected. However, if the climate-driven changes are strongly affected by the redistribution of heat and carbon, then thermal and acidifying events are more likely to occur in isolation of each other.

Our study has focused on the dynamic redistribution acting on a horizontal scale of many thousands of kilometers, but this dynamic redistribution may also be important on a finer scale of eastern boundary upwelling events or ocean mesoscale eddies, where again a horizontal and vertical redistribution of the pre-existing thermal and carbon anomalies are likely to lead to opposite-signed contributions. Finally, more mechanistic insight may be gained into the ongoing imprint of climate change and its likely future effect by assessing how these thermal and acidifying events are connected to the addition and redistribution of heat and carbon.

Acknowledgments. The authors acknowledge the World Climate Research Programme's Working Group on Coupled Modelling responsible for CMIP, together with support and

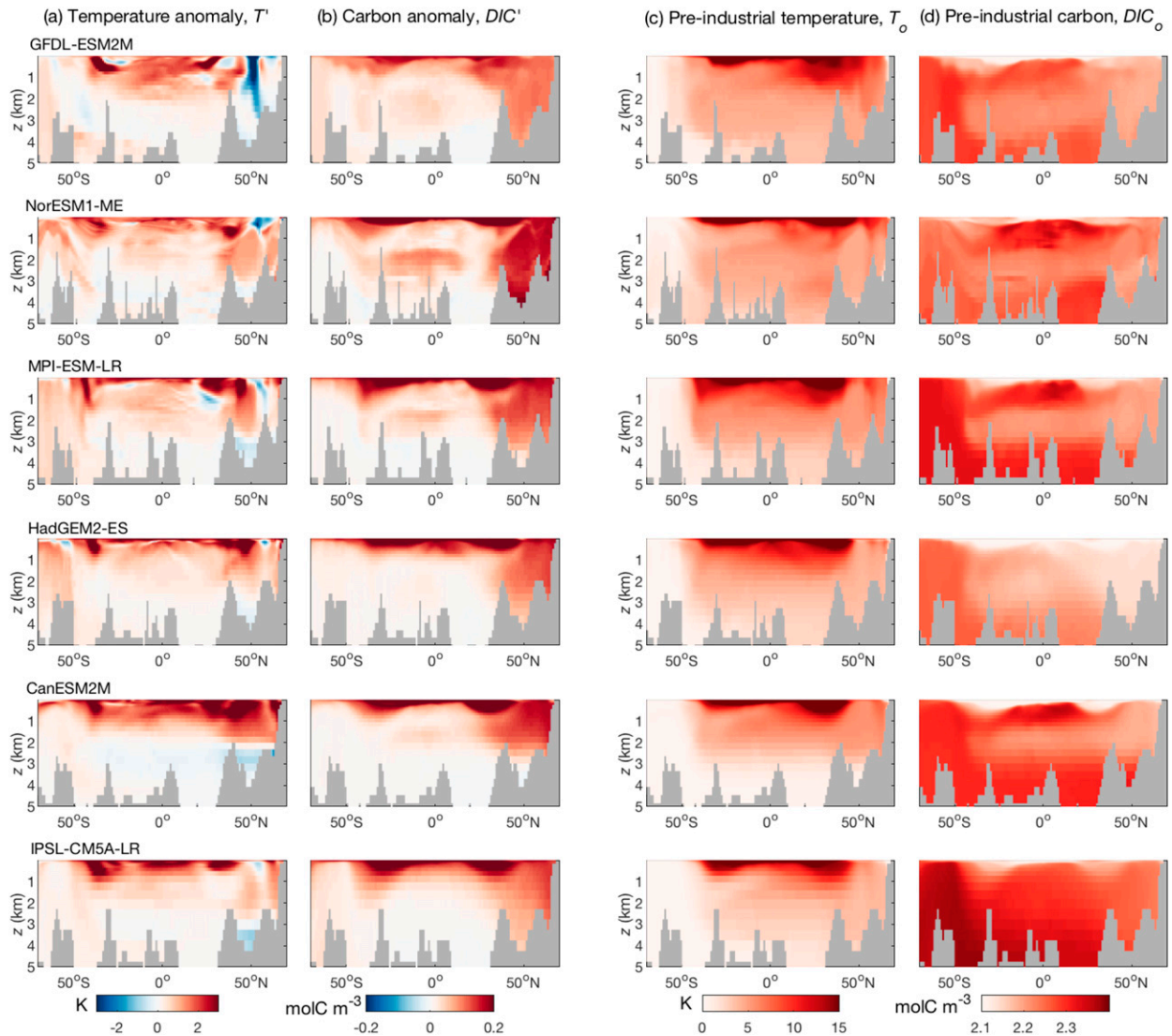


FIG. A1. Meridional sections for the modeled change over the Atlantic sectors along 32°W for temporal changes in (a) temperature T' (K) and (b) dissolved inorganic carbon DIC' (mol C m^{-3}) for years 100–140 for an annual 1% increase in CO_2 projections, which are relative to the preindustrial (c) temperature T_0 (K) and (d) dissolved inorganic carbon DIC_0 (mol C m^{-3}) for GFDL-ESM2M, NorESM1-ME, MPI-ESM-LR, HadGEM2-ES, CanESM2M, and IPSL-CM5A-LR.

software development by the U.S. Department of Energy Program for Climate Model Diagnosis and Intercomparison, and the Global Organisation for Earth System Science Portals. We acknowledge support from the U.K. Natural Environmental Research Council (NE/T007788/1, NE/T010657/1). We thank Andy Watson for discussions about the wider carbon context and are grateful to three referees for raising detailed and constructive points that strengthened the manuscript.

Data availability statement. The data that support the findings of this study are openly available. The data input files are all based upon CMIP data that are available from the Earth System Grid Federation at <https://esgf-node.llnl.gov/projects/esgf-llnl/>.

APPENDIX

Anthropogenic and Preindustrial Temperature and Carbon for the Atlantic Ocean

The meridional structure of the anthropogenic temperature and carbon distributions from the Earth system model projections are broadly similar to each other on the basin scale, illustrated here for the Atlantic basin (Figs. A1a,b). Their distributions follow expected ventilation pathways with enhanced tracer values within the surface mixed layer and the thermocline, particularly within the centers of the subtropical gyres at typically 30°N and 30°S , and within the high latitudes of the North Atlantic. There are larger intermodel differences in

anthropogenic temperature distributions in the high latitudes of the North Atlantic and Southern Ocean (Fig. A1a), and some intermodel differences in the anthropogenic carbon below the thermocline in the tropical Atlantic (Fig. A1b).

There are similar preindustrial temperature distributions in each of the models (Fig. A1c), but a wider range in the preindustrial carbon distributions (Fig. A1d) with HadGEM2-ES having a relatively weak vertical gradient over the North Atlantic. Over most of the domain, the vertical gradient for preindustrial temperature and carbon are of the opposite sign.

REFERENCES

- Armour, K. C., J. Marshall, J. R. Scott, A. Donohoe, and E. R. Newsom, 2016: Southern Ocean warming delayed by circumpolar upwelling and equatorward transport. *Nat. Geosci.*, **9**, 549–554, <https://doi.org/10.1038/ngeo2731>.
- Arora, V. K., and Coauthors, 2011: Carbon emission limits required to satisfy future representative concentration pathways of greenhouse gases. *Geophys. Res. Lett.*, **38**, L05805, <https://doi.org/10.1029/2010GL046270>.
- , and Coauthors, 2020: Carbon–concentration and carbon–climate feedbacks in CMIP6 models and their comparison to CMIP5 models. *Biogeosciences*, **17**, 4173–4222, <https://doi.org/10.5194/bg-17-4173-2020>.
- Banks, H. T., and J. M. Gregory, 2006: Mechanisms of ocean heat uptake in a coupled climate model and the implications for tracer based predictions of ocean heat uptake. *Geophys. Res. Lett.*, **33**, L07608, <https://doi.org/10.1029/2005GL025352>.
- Bernardello, R., I. Marinov, J. B. Palter, J. L. Sarmiento, E. D. Galbraith, and R. D. Slater, 2014: Response of the ocean natural carbon storage to projected twenty-first-century climate change. *J. Climate*, **27**, 2033–2053, <https://doi.org/10.1175/JCLI-D-13-00343.1>.
- Bronseleer, B., and L. Zanna, 2020: Heat and carbon coupling reveals ocean warming due to circulation changes. *Nature*, **584**, 227–233, <https://doi.org/10.1038/s41586-020-2573-5>.
- Clement, D., and N. Gruber, 2018: The eMLR (C*) method to determine decadal changes in the global ocean storage of anthropogenic CO₂. *Global Biogeochem. Cycles*, **32**, 654–679, <https://doi.org/10.1002/2017GB005819>.
- DeVries, T., 2014: The oceanic anthropogenic CO₂ sink: Storage, air–sea fluxes, and transports over the industrial era. *Global Biogeochem. Cycles*, **28**, 631–647, <https://doi.org/10.1002/2013GB004739>.
- , M. Holzer, and F. Primeau, 2017: Recent increase in oceanic carbon uptake driven by weaker upper-ocean overturning. *Nature*, **542**, 215–218, <https://doi.org/10.1038/nature21068>.
- Dufresne, J.-L., and Coauthors, 2013: Climate change projections using the IPSL-CM5 Earth system model: From CMIP3 to CMIP5. *Climate Dyn.*, **40**, 2123–2165, <https://doi.org/10.1007/s00382-012-1636-1>.
- Dunne, J. P., and Coauthors, 2013: GFDL’s ESM2 global coupled climate–carbon Earth system models. Part II: Carbon system formulation and baseline simulation characteristics. *J. Climate*, **26**, 2247–2267, <https://doi.org/10.1175/JCLI-D-12-00150.1>.
- Follows, M. J., T. Ito, and S. Dutkiewicz, 2006: On the solution of the carbonate chemistry system in ocean biogeochemistry models. *Ocean Modell.*, **12**, 290–301, <https://doi.org/10.1016/j.ocemod.2005.05.004>.
- Friedlingstein, P., and Coauthors, 2006: Climate–carbon cycle feedback analysis: Result from the C⁴MIP model intercomparison. *J. Climate*, **19**, 3337–3353, <https://doi.org/10.1175/JCLI3800.1>.
- , and Coauthors, 2020: Global carbon budget 2020. *Earth Syst. Sci. Data*, **12**, 3269–3340, <https://doi.org/10.5194/essd-12-3269-2020>.
- Frölicher, T. L., and C. Laufkötter, 2018: Emerging risks from marine heat waves. *Nat. Commun.*, **9**, 650, <https://doi.org/10.1038/s41467-018-03163-6>.
- , J. L. Sarmiento, D. J. Paynter, J. P. Dunne, J. P. Krasting, and M. Winton, 2015: Dominance of the Southern Ocean in anthropogenic carbon and heat uptake in CMIP5 models. *J. Climate*, **28**, 862–886, <https://doi.org/10.1175/JCLI-D-14-00117.1>.
- , E. M. Fischer, and N. Gruber, 2018: Marine heatwaves under global warming. *Nature*, **560**, 360–364, <https://doi.org/10.1038/s41586-018-0383-9>.
- Giorgetta, M. A., and Coauthors, 2013: Climate and carbon cycle changes from 1850 to 2100 in MPI-ESM simulations for the Coupled Model Intercomparison Project phase 5. *J. Adv. Model. Earth Syst.*, **5**, 572–597, <https://doi.org/10.1002/jame.20038>.
- Gnanadesikan, A., 1999: A simple predictive model of the structure of the oceanic pycnocline. *Science*, **283**, 2077–2079, <https://doi.org/10.1126/science.283.5410.2077>.
- Gregory, J. M., and Coauthors, 2004: A new method for diagnosing radiative forcing and climate sensitivity. *Geophys Res Lett.*, **31**, L03205, <https://doi.org/10.1029/2003GL018747>.
- , and Coauthors, 2016: The Flux-Anomaly-Forced Model Intercomparison project (FAFMIP) contribution to CMIP6: Investigation of sea-level and ocean climate change in response to CO₂ forcing. *Geosci. Model Dev.*, **9**, 3993–4017, <https://doi.org/10.5194/gmd-9-3993-2016>.
- Gruber, N., 2011: Warming sour, turning sour, losing breath: Ocean biogeochemistry under global change. *Philos. Trans. Roy. Soc. London*, **369A**, 1980–1996, <https://doi.org/10.1098/rsta.2011.0003>.
- , J. L. Sarmiento, and T. F. Stocker, 1996: An improved method for detecting anthropogenic CO₂ in the oceans. *Global Biogeochem. Cycles*, **10**, 809–837, <https://doi.org/10.1029/96GB01608>.
- , P. Landschützer, and N. S. Lovenduski, 2019: The variable Southern Ocean carbon sink. *Annu. Rev. Mar. Sci.*, **11**, 159–186, <https://doi.org/10.1146/annurev-marine-121916-063407>.
- Hall, T. M., T. W. Haine, and D. W. Waugh, 2002: Inferring the concentration of anthropogenic carbon in the ocean from tracers. *Global Biogeochem. Cycles*, **16**, 1131, <https://doi.org/10.1029/2001GB001835>.
- Jones, C. D., and Coauthors, 2011: The HadGEM2-ES implementation of CMIP5 centennial simulations. *Geosci. Model Dev.*, **4**, 543–570, <https://doi.org/10.5194/gmd-4-543-2011>.
- Katavouta, A., R. G. Williams, and P. Goodwin, 2019: The effect of ocean ventilation on the transient climate response to emissions. *J. Climate*, **32**, 5085–5105, <https://doi.org/10.1175/JCLI-D-18-0829.1>.
- Khatiwal, S., F. Primeau, and T. Hall, 2009: Reconstruction of the history of anthropogenic CO₂ concentrations in the ocean. *Nature*, **462**, 346–349, <https://doi.org/10.1038/nature08526>.
- Marshall, D. P., and L. Zanna, 2014: A conceptual model of ocean heat uptake under climate change. *J. Climate*, **27**, 8444–8465, <https://doi.org/10.1175/JCLI-D-13-00344.1>.
- Marshall, J., J. R. Scott, K. C. Armour, J.-M. Campin, M. Kelley, and A. Romanou, 2015: The ocean’s role in the transient response of climate to abrupt greenhouse gas forcing. *Climate Dyn.*, **44**, 2287–2299, <https://doi.org/10.1007/s00382-014-2308-0>.
- Myrhe, G., E. J. Highwood, K. P. Shine, and F. Stordal, 1998: New estimates of radiative forcing due to well mixed greenhouse

- gases. *Geophys. Res. Lett.*, **25**, 2715–2718, <https://doi.org/10.1029/98GL01908>.
- Resplandy, L., and Coauthors, 2018: Revision of global carbon fluxes based on a reassessment of oceanic and riverine carbon transport. *Nat. Geosci.*, **11**, 504–509, <https://doi.org/10.1038/s41561-018-0151-3>.
- Sabine, C. L., and Coauthors, 2004: The oceanic sink for anthropogenic CO₂. *Science*, **305**, 367–371, <https://doi.org/10.1126/science.1097403>.
- Schwinger, J., and Coauthors, 2014: Nonlinearity of ocean carbon cycle feedbacks in CMIP5 Earth system models. *J. Climate*, **27**, 3869–3888, <https://doi.org/10.1175/JCLI-D-13-00452.1>.
- Thomas, J., D. Waugh, and A. Gnanadesikan, 2018: Relationship between ocean carbon and heat multidecadal variability. *J. Climate*, **31**, 1467–1482, <https://doi.org/10.1175/JCLI-D-17-0134.1>.
- Tjiputra, J. F., C. Roelandt, M. Bentsen, D. M. Lawrence, T. Lorentzen, J. Schwinger, O. Seland, and C. Heinze, 2013: Evaluation of the carbon cycle components in the Norwegian Earth System Model (NorESM). *Geosci. Model Dev.*, **6**, 301–325, <https://doi.org/10.5194/gmd-6-301-2013>.
- Waugh, D., T. Hall, B. McNeil, R. Key, and R. Matear, 2006: Anthropogenic CO₂ in the oceans estimated using transit time distributions. *Tellus*, **58B**, 376–389, <https://doi.org/10.1111/j.1600-0889.2006.00222.x>.
- Williams, R. G., A. Katavouta, and P. Goodwin, 2019: Carbon-cycle feedbacks operating in the climate system. *Curr. Climate Change Rep.*, **5**, 282–295, <https://doi.org/10.1007/s40641-019-00144-9>.
- Winton, M., S. M. Griffies, B. L. Samuels, J. L. Sarmiento, and T. L. Frölicher, 2013: Connecting changing ocean circulation with changing climate. *J. Climate*, **26**, 2268–2278, <https://doi.org/10.1175/JCLI-D-12-00296.1>.
- Xie, P., and G. K. Vallis, 2012: The passive and active nature of ocean heat uptake in idealized climate change experiments. *Climate Dyn.*, **38**, 667–684, <https://doi.org/10.1007/s00382-011-1063-8>.
- Zanna, L., S. Khatiwala, J. M. Gregory, J. Ison, and P. Heimbach, 2019: Global reconstruction of historical ocean heat storage and transport. *Proc. Natl. Acad. Sci. USA*, **116**, 1126–1131, <https://doi.org/10.1073/pnas.1808838115>.